Dalton Transactions

Accepted Manuscript

This is an *Accepted Manuscript*, which has been through the Royal Society of Chemistry peer review process and has been accepted for publication.

Accepted Manuscripts are published online shortly after acceptance, before technical editing, formatting and proof reading. Using this free service, authors can make their results available to the community, in citable form, before we publish the edited article. We will replace this *Accepted Manuscript* with the edited and formatted *Advance Article* as soon as it is available.

You can find more information about *Accepted Manuscripts* in the Information for Authors.

Please note that technical editing may introduce minor changes to the text and/or graphics, which may alter content. The journal's standard Terms & Conditions and the Ethical guidelines still apply. In no event shall the Royal Society of Chemistry be held responsible for any errors or omissions in this *Accepted Manuscript* or any consequences arising from the use of any information it contains.

ROYAL SOCIETY OF CHEMISTRY

www.rsc.org/dalton

Surface Plasmon Resonance Effect for the Enhancement of Photodegradation Activity by Au/$ZnSn(OH)_6$ Nanocubes

Jyh Ming Wu * and Yu Nong Chen

Department of Materials Science and Engineering, National Tsing Hua University, 101, Section 2 Kuang Fu Road, Hsinchu 300.

E-mail wujm@mx.nthu.edu.tw

Abstract

We demonstrated the Au/$ZnSn(OH)_6$ hollow nanocubes that exhibited extremely high photodegradation activity under ultraviolet and visible-light illumination. The pristine $ZnSn(OH)_6$ hollow nanocubes can achieve 100% photodegradation ratio within 20 mins under ultraviolet-light illumination. The high photodegradation activity of the $ZnSn(OH)_6$ can be attributed to a plenty of OH groups in presence of the polyhedral corner of the $ZnSn(OH)_6$ to generate a large number of reactive hydroxyl radicals for degradation of dye moleculer. High resolution transmission electron microscopy (HRTEM) and scanning electron microscopy (SEM) images revealed that the size of the $ZnSn(OH)_6$ and Au/$ZnSn(OH)_6$ hollow nanocubes is ~ 30-80 nm. After Au decorated $ZnSn(OH)_6$ nanocubes, the heterostructures have exhibited a significance of strong and widen absorption peak in 450-750 nm because of surface plasmon resonance (SPR) effect, which therefore showed an excellent photodegradation activity under visible-light illumination. The rate constant k of Au/$ZnSn(OH)_6$ is as high as 51.8 $L\ mole^{-1}\ min^{-1}$ under UV-light illumination. This value is much higher than those in the previous reports so far. The hydroxyl groups essentially enhances the reaction rate and forms the active radicals to participate in the reaction for destruction of the Rhodamine B (RB) solution. The Au/$ZnSn(OH)_6$ has been successfully applied for hybrid coating screen with polydimethylsiloxan (PDMS), which exhibited an excellent mechanical desirable durability and extended its feasible application in our daily life.

Dalton Transactions Accepted Manuscript

1. Introduction

The semiconductor nanostructures are offering a promising future in many fields, such as energy, optoelectronics, photocatalysis, and light emission etc. Of the semiconductor nanomaterials, the ZnO[1] and TiO_2[2-4] have extensively studied in the dissociation of organic compounds, microbial disinfection byproducts, and contaminants from water and air.[5] The enormous efforts have been devoted to these nanomaterials in photoelectrochemical areas, which has led to many prospective applications in areas ranging from photodevices to photocatalysis and antimicrobial peptides.[2] The ZnO[6] and TiO_2[7, 8] materials does not respond to visible light owing to its large band gap (~3.2-3.2 eV), although there have many methodologies to be developed to improve their photocatalytic activity by doping with metal transition ions[9] and/or incorporated with surface defects[10, 11] etc. However, the photoinduced carrier recombination in semiconductor materials could cause the low photocatalytic activity, which may contribute to one of the most critical problems for prohibiting commercial applications of photocatalysis.

Recently, a non-toxicity of $ZnSn(OH)_6$ nanocubes was reported to have higher photocatalytic activity under UV-light irradiation in addition to TiO_2 and ZnO nanostructures. However, it is very important to develop the high photocatalytic activity of nanomaterials under visible-light illumination for commercial applications.[12] There have many reports to discuss on the surface plasmon absorption of Au nanoparticles (NPs) decorated TiO_2[13] and ZnO[14] nanowires or nanoparticles, which have been evidenced to improve their photocatalytic activity, but there is no report on visible light-driven surface plasmonic photocatalyst of the $Au/ZnSn(OH)_6$ heterojunction nanocubes. The surface plasmon resonance (SPR) is attributed to that the collective oscillations of valence electrons take place due to the incoming photons. When the frequency of incoming light matches with the frequency of surface's free electrons oscillating against the restoring force of the positive nuclei and occurs a resonant phenomenon.[15] Such electron transfer would greatly enhance the separation of photogenerated electron-hole pairs and therefore improve the photocatalytic

Dalton Transactions Accepted Manuscript

activity under visible-light illumination[16].

This work, an ion-exchange method was employed to synthesize the hollow-like $ZnSn(OH)_6$ and $Au/ZnSn(OH)_6$ heterojunction nanocubes. The photodegradation ratio of $ZnSn(OH)_6$ hollow nanocubes can be reached 100% within 20 minute under ultraviolet-light irradiation. Due to a large number of OH groups in presence of the $ZnSn(OH)_6$, which can be regarded as a mediation for the destruction of organics on the $ZnSn(OH)_6$ by producing H_2O_2 and OH radicals species. After Au decorated the $ZnSn(OH)_6$ nanocubes, the nanocubes have therefore showed a significant absorption peak in the range of 450-750 nm, which suggested a surface plasmon resonance (SPR) effect.

The SPR effect and high concentration of OH groups exhibited the high stability and photocatalytic activity of the $Au/ZnSn(OH)_6$ nanocubes in contrast to the pristine $ZnSnO_3$ and $ZnSn(OH)_6$ nanocubes under visible-light irradiation. This is the first comprehensive report on the photocatalytic activity with a combination of SPR effect through $Au/ZnSn(OH)_6$ nanocubes. The specific rate constant k of the $ZnSn(OH)_6$ nanocubes under UV-light illumination is as high as 51.8 $L\,mole^{-1}$ min^{-1}. This value is much higher than those in the previous reports.[17-20] The $Au/ZnSn(OH)_6$ can be implanted on a PDMS-coated window screen to form a hybrid coating screen ($PDMS\text{-}Au/ZnSn(OH)_6$), which exhibited excellent mechanical desirable durability for decolorization of RB dyes under the UV and/or visible-light illumination.

2. Experimental sections

Materials Synthesis

The source materials of $Na_2SnO_3{\bullet}3H_2O$ (0.534 g) and $Zn(CH_3COO)_2{\bullet}3H_2O$ (0.439 g) were dissolved in ethylene glycol and deionized water solution to obtain aqueous solutions. The Na_2SnO_3 solution was added dropwise to the $Zn(CH_3COO)_2$ solution under magnetic stirring at room temperature for 10 minutes, and yielded a precipitate of $ZnSn(OH)_6$ in white color. The precipitate $ZnSn(OH)_6$ nanocubes was then collected by centrifugation and washed by 5 times using deionized water. After that, as-prepared product was dried at 100°C to prepare the nanocubes. After annealing the $ZnSn(OH)_6$ nanocubes at 400°C for 1hr, an amorphous $ZnSnO_3$ nanocubes were therefore

Dalton Transactions Accepted Manuscript

synthesized. To prepare Au NPs decorated $ZnSn(OH)_6$ nanocubes, the $ZnSn(OH)_6$ nanocubes was dispersed in 0.01M $HAuCl_4$ solution and stirred for 2 hours at 70°C. After drying the reactant at 80°C, the reactant was then annealed at 150°C to produce the Au/$ZnSn(OH)_6$ nanocubes. Similarly, the Au NPs decorated $ZnSnO_3$ nanocubes was obtained by annealing Au/$ZnSn(OH)_6$ nanocubes at 400 °C.

Materials Characterization

As-prepared nanocubes were measured by thin film x-ray diffractometer (Burker D2) and high-resolution transmission electron microscope (HRTEM, JEOL JEM-ARM200FTH) to investigate their crystal structure. The field emission scanning electron microscopy (FESEM, Hitachi SU8010) was employed to investigate the morphologies of nanocubes. The chemical nature of the nanocubes was investigated by high-resolution X-ray photoelectron spectroscopy (ULVAC-PHI PHI 5000 Versaprobe II). The Rhodamine B (RhB) aqueous solution (10 ppm) was used to evaluate photodegradation activity under UV-light (wavelength > 254nm) and visible-light (wavelength > 450 nm) illumination. The optical properties of as-synthesized nanocubes were measured by UV-vis spectrophotometers (Hitachi, U-3900), photoluminescence, and Raman spectroscopy (Horiba Jobin Yvon, HR 550 with a deep UV laser 266 nm). The Horiba fluoromax-4 spectrofluorometer was used to measure the fluorescent property of as-prepared nanocubes mixing with terephthalic acid solution under visible-light illumination to investigate the concentration of $^{\bullet}OH$ radicals.[21]

3. Results and Discussion

Figure 1a shows that as-synthesized products naturally formed polyhedral nanocrystals with systematic cube-shaped morphology. The size of nanocube is in the range of 30-80 nm. After annealing the nanocubes at 400 °C for 1 h in air, the cube-shaped does not change significantly, as shown in Figure 1b. The x-ray diffraction patterns in Figure 1c shows that these cube-shaped nanocrystallines belong to $ZnSn(OH)_6$ (JCPDS card no. 20-1455, a = b = c = 7.8Å, space group:

Dalton Transactions Accepted Manuscript

$Pn\bar{3}m$).[22] The $ZnSn(OH)_6$ nanocubes became amorphous structure after annealed them at 400 ^oC for 1 hr, as shown the lower XRD pattern in Figure 1c. Micro-Raman was used to further verify the amorphous nanocrystallines. Figure 1d (lower spectrum) reveals three Raman characteristic peaks of the $ZnSn(OH)_6$ at 298, 371, and 607 cm^{-1}, which confirmed the structure of $ZnSn(OH)_6$. The peak at 298 cm^{-1} can be attributed to the M-Zn-M (M: Zn or Sn) of bending vibration modes while the peak at 607 cm^{-1} is ascribed to M−OH stretching vibrations modes. In contrast, Figure 1d (upper spectrum) reveals two Raman characteristic modes at 547 and 664 cm^{-1}, further confirms that the cube-shaped amorphous structure is $ZnSnO_3$ phase,[23] as govern by the following chemical reaction.[23]

$$ZnSn(OH)_6 \rightarrow ZnSnO_3 + 3H_2O \quad (1)$$

The crystallographic $ZnSn(OH)_6$ and $ZnSnO_3$ are shown in Figure 2b and 2c, respectively. Among them, there are no significant differences in their crystal structures. The $ZnSn(OH)_6$ consisted of two octahedral cells such as $Zn(OH)_6$ and $Sn(OH)_6$.[24] The Sn and Zn ion position at a equivalent in the $Sn(OH)_6$ and $Zn(OH)_6$ octahedral cells, respectively. The framework of $ZnSn(OH)_6$ share their O-H in the corner-site of each polyhedral cell while that of $ZnSnO_3$ share their O in the same corner to bulit-in the framework of the $ZnSn(OH)_6$ and $ZnSnO_3$ crystal structure.

The low-magnitude TEM image in Figure 3a-3b clearly exhibited the $ZnSn(OH)_6$ hollow structure. The nanocubes has an average edge length of ~ 50 nm. Figure 3c reveals that most of the nanocubes are individually separated from each other. Figure 3d shows the lattice fringe of 0.392 nm, which is corresponding to (200) plane of $ZnSn(OH)_6$. The fast Fourier transforms (FFT) image is shown in the inset image in Figure 3d, which evidenced that the $ZnSn(OH)_6$ nanocube is quasi-single crystal structure. After annealing the $ZnSn(OH)_6$ at 400^oC, Figure 3e and its inset image show that the size of $ZnSnO_3$ nanocubes is still in the range of 30-80 nm. There is no significant difference in the dimensions and morphology if compare with the $ZnSn(OH)_6$ nanocubes. The hollow structure of $ZnSnO_3$ nanocubes is observed by the inset image of Figure 3e. Figure 3f

Dalton Transactions Accepted Manuscript

(FFT image) further shows that the $ZnSnO_3$ nanocubes are amorphous structure. As-prepared $ZnSn(OH)_6$ nanocubes was then dispersed in 0.01M $HAuCl_4$ solution to synthesize the Au NPs decorated with $ZnSn(OH)_6$ nanocubes. Figure 3g shows that the Au NPs are uniformly deposited on the surface of the $ZnSn(OH)_6$ and forms heterojunction nanocubes. Figure 3h further reveals that the size of single crystal Au NPs is around 3-5 nm with a lattice spacing of ~ 0.233 nm.

The photocatalytic activities were investigated by immersing the $ZnSn(OH)_6$, $ZnSnO_3$, $Au/ZnSn(OH)_6$, and $Au/ZnSnO_3$ nanocubes into Rhodamine B (RB, 10 ppM) solution. Figures 4a-4d show the absorbance ratios with respect to the wavelength under $ZnSnO_3$, $Au/ZnSnO_3$, $ZnSn(OH)_6$, and $Au/ZnSn(OH)_6$ nanocubes with RB dye solution, respectively. The photodegradation efficiency of the $ZnSn(OH)_6$ and $Au/ZnSn(OH)_6$ nanocubes are much better than those of the $ZnSnO_3$ and $Au/ZnSnO_3$ nanocubes. Figure 5a further reveals that the RB dye molecular is fully degradated in 20 mins by the $ZnSn(OH)_6$ and $Au/ZnSn(OH)_6$ nanocubes. The degradation rate of the $Au/ZnSn(OH)_6$ is faster than that of $ZnSn(OH)_6$ before ten minutes, however, after that, the degradation rate of the $ZnSn(OH)_6$ is slightly higher than that of $Au/ZnSn(OH)_6$. After five photocatalytic cycling tests using the $ZnSn(OH)_6$ nanocubes, the rate of color lost was still 100% of the initial rate within 20 mins, as shown in Figure 5b. The repeated tests demonstrated high stability of the $ZnSn(OH)_6$ catalyst in the reaction medium without observable loss of photocatalytic activity. To the best of our knowledge, this is the best photodegradation ratio under UV-light irradiation using $ZnSn(OH)_6$.

To understand the possible mechanism of the high photocatalytic activity of $ZnSn(OH)_6$, further optical and chemical species were carried out by PL and XPS, respectively. On the basis of our photoluminescence (PL) spectra in Figure 5c, a board green-yellow emission band of $ZnSn(OH)_6$ and $ZnSnO_3$ is centered at 500 nm and 610 nm, respectively. The PL intensity of the $ZnSn(OH)_6$ is much lower than that of the $ZnSnO_3$ nanocubes. The result imply that the $ZnSn(OH)_6$ nanocubes exhibited a enhancement of the charge separation efficiency of photogenerated electron−hole pairs in contrast to $ZnSnO_3$ nanocubes. What's more, the O1s peaks of $ZnSnO_3$ and

Dalton Transactions Accepted Manuscript

$ZnSn(OH)_6$ in Figure 5d further reveal that the OH group's intensity of the $ZnSn(OH)_6$ is much higher than that of the $ZnSnO_3$ nanocubes. The high photocatalytic activity can be explained by the following chemical reactions. First, the UV-light induced electron-hole pair separations in $ZnSn(OH)_6$ nanocubes (see reaction (2)). Next, the M-OH recombine with hole to generate hydroxyl radical ($OH^{\cdot}$) with M^+, as shown in reaction (3). Where M^+ denotes Sn or Zn ion. The electron migrated to the surface of $ZnSn(OH)_6$ to form oxygen ions (O_2^-), which reacted with H^+ to produce the hydrogen peroxide (H_2O_2) (see reaction 4). The hydrogen peroxide was dissociated into hydroxyl radical ($OH^{\cdot}$) under UV irradiation, as shown in reaction (5). The hydroxyl radicals are highly active chemical species to dissociate the dye molecular.

$$ZnSn(OH)_6 + hv \rightarrow e^- + h^+ \quad (2)$$

$$M-OH + h^+ \rightarrow OH^{\cdot} + M^+ \quad (3)$$

$$e^- + O_2^- + 2H^+ \rightarrow H_2O_2 \quad (4)$$

$$H_2O_2 + hv \rightarrow 2OH^{\cdot} \quad (5)$$

To extend its absorption range from UV to visible-light illumination, the $ZnSnO_3$, $ZnSn(OH)_6$, $Au/ZnSnO_3$, and $Au/ZnSn(OH)_6$ nanocubes were immersed in RB solution to investigate their surface plasmon resonance effect. Figure 6a-6d shows the absorbance ratios with respect to the wavelength under RB with $ZnSnO_3$, RB with $Au/ZnSnO_3$, RB with $ZnSn(OH)_6$, and RB with $Au/ZnSn(OH)_6$ nanocubes, respectively. Among them, the RB with $Au/ZnSn(OH)_6$ nanocubes exhibited the highest photodegradation ratio ranging from 0 to 120 min under visible-light irradiation, as shown in Figure 6e. The photodegradation activity is following the order: $Au/ZnSn(OH)_6 > Au/ZnSnO_3 > ZnSn(OH)_6 > ZnSnO_3$. However, Figure 6f clearly shows that the absorbance intensity increased in the following order: $Au/ZnSnO_3 > Au/ZnSn(OH)_6 > ZnSn(OH)_6 > ZnSnO_3$. A broad peak over the 450-750 nm range can be ascribed to the surface plasmon resonance effect. The photodegradation activity is not follows the same order as shown in their absorbance spectra, implied that some critical factors may dominate the photocatalytic activity for these nanocubes. We suggested that there have two important factors may be possible responsible for the

Dalton Transactions Accepted Manuscript

high photodegradation activity of the Au/$ZnSn(OH)_6$ heterojunction nanocubes. The first one is the OH groups in $ZnSn(OH)_6$ nanocubes. On the basis of the PL spectra of the $ZnSn(OH)_6$ and $ZnSnO_3$ nanocubes, the PL intensity of $ZnSn(OH)_6$ greatly decreased in contrast to that of $ZnSnO_3$ nanocubes. The OH groups can efficient act as a trapping centers to reduce recombination rate of the photogenerated electron-hole pairs. The second reason is due to the surface plasmon absorption of Au NPs, which can be took advantage of the $ZnSn(OH)_6$ catalyst under visible-light irradiation.[25] Because a plenty of electrons was filled in d-band of Au below Fermi level, the photogenerated electron are excited to the high energy level of gold and transferred to the conduction band of the $ZnSn(OH)_6$ nanocubes by interband transitions. This is due to the existence of electric field at the metal-semiconductor heterojunction between Au and $ZnSn(OH)_6$.[26]

The electrons in the conduction band of $ZnSn(OH)_6$ can generate superoxide radicals to dissociate the dye molecular to enhance photocatalytic activity (see working mechanism below). Accordingly, Au/$ZnSn(OH)_6$ heterojunction nanocubes exhibited the highest photodegradation activity under visible-light irradiation. The observed rate constant of the Au/$ZnSn(OH)_6$ under UV-light illumination, k_{obs}, was verified from the pseudo first-order reaction, as determined from Equ. (6).[21] The k_{obs} of Au/$ZnSn(OH)_6$ nanocubes under UV-light illumination is 0.18 min^{-1}. The specific rate constant k was further determined from the Equ. (7), which equals to 51.8 $L\ mole^{-1}$ min^{-1}. This value is much higher than those in the previous reports.[17-19] Where C_o and C_t is the concentration at time = 0 and time = t, respectively. [M] denotes the concentration of nanocubes. Moreover, the rate constant k of the Au/$ZnSn(OH)_6$ under visible-light illumination is 1.62×10^{-8} $mole$ L^{-1} min^{-1}, as calculated from the slope of the zero-order kinetic reaction (Equ. (8)) and the concentration of RB dye (eg., 10ppm).

$$ln\frac{[C_0]}{[C_t]} = k_{obs} \cdot t \qquad (6)$$

$$\frac{k_{obs}}{[M]} = k \qquad (7)$$

$$\frac{[C_t]-[C_0]}{t} = k \qquad (8)$$

Dalton Transactions Accepted Manuscript

The schematic diagram is shown in Figure 7 to explain the working mechanism of high photocatalytic activity of the Au/$ZnSn(OH)_6$ nanocubes. Under UV-light irradiation, the electron is excited from the valence band to the conduction band of the $ZnSn(OH)_6$, the electrons migrated to the surface of the $ZnSn(OH)_6$ and reacted with oxygen to form oxygen radicals ($\cdot O$-), as shown the route A in Figure 7a. As a consequence, the remaining hole was reacted with OH groups in $ZnSn(OH)_6$ to generate the hydroxyl radicals. In contrast, the route B in Figure 7a depicts that photoexcited electrons in the Au/$ZnSn(OH)_6$ move into the conduction band of $ZnSn(OH)_6$. The electrons in the conduction band of $ZnSn(OH)_6$ can generate superoxide radicals to dissociate the dye molecular. The Au NPs can be regarded as an quencher of photoexcited $ZnSn(OH)_6$ nanocubes and accepting electrons from the conduction band of $ZnSn(OH)_6$. Namely, Au NPs may act as a trapping site of electron to decrease the recombination rate so that the photogenerated electron can migrate from the conduction band of $ZnSn(OH)_6$ to Au NPs to participate in photocatalytic reactions. Accordingly, Au/$ZnSn(OH)_6$ heterojunction nanocubes exhibited the highest photodegradation activity under UV-light illumination. Similarly, we have observed the same effect in the Au/$ZnSnO_3$ nanocubes, which photocatalytic activity is however much lower than that of Au/$ZnSn(OH)_6$ because of less OH groups. We therefore suggested that each octahedral cell of $M(OH)_6$ (M: Zn or Sn) possesses four OH ions that positions at its corner-site, which may be responsible for their high photodegradation activity in the destruction of RB solution.[18]

Figure 7b schematically depicted the SPR effect of Au/$ZnSn(OH)_6$ nanocubes.[27] First, Au-NPs can capture electrons from the organic molecules adsorbed on them due to its high electronegativity.[28] The gold NPs therefore absorbed the visible-light and excited the electrons from low energy levels to high energy levels via interband transitions of the 6 sp electrons of gold.[29] Next, because an electric field was established between Au and $ZnSn(OH)_6$, the electrons therefore migrated from the high energy state of Au to the conduction band of the $ZnSn(OH)_6$ to react with oxygen and formed oxygen radicals. In addition, there have many defects states formed on the surface of Au/$ZnSn(OH)_6$, as shown in PL spectra (see Figure 5c). The electrons in defect levels can

Dalton Transactions Accepted Manuscript

be excited by visible-light, leading to the electron reacted with oxygen to reproduce the active radicals of oxygen. Meanwhile, the remaining hole was reacted with the OH groups in $ZnSn(OH)_6$ to regenerate the hydroxyl radicals. Thus, the hydroxyl groups essentially enhances the reaction rate and forms the active radicals, such as oxygen radicals and hydroxyl radicals to participate in the reaction for destruction of the RB solution.

To confirm the enhancement of photocatalytic activity of Au decorated nanocubes is attributed to SPR effect, the terephthalic acid ($C_8H_6O_4$, 5×10^{-4} M) was mixed with sodium hydroxide (NaOH, 2×10^{-3} M) to prepare the colorless aqueous solution.[30] The $ZnSn(OH)_6$, $ZnSn(OH)_3$, $Au/ZnSn(OH)_6$, and $Au/ZnSnO_3$ nanocubes were individually immersing in the diluted terephthalic acid solution under visible-light illumination for 0, 20, 40, 60, 80, 100, and 120 minutes to observe their $^{\bullet}OH$ radicals' concentration, as generated by SPR effect. It should be noted that the $^{\bullet}OH$ radicals were formed when the nanocubes were immersed in terephthalic acid solution under visible-light illumination. The 2-hydroxyterephthalic acid was then produced in the solution when the terephthalic acid was reacted with $^{\bullet}OH$ radicals. The emission band of 2-hydroxyterephthalic acid is expected to be located in the range of 420-440 nm. After illuminated these hybrid solutions under visible-light for 0, 20, 40, 60, 80, 100, and 120 minutes, Figures 8a-8d show the fluorescent intensity as a function of wavelength for $ZnSn(OH)_6$, $ZnSnO_3$, $Au/ZnSn(OH)_6$, and $ZnSnO_3$ nanocubes mixing with terephthalic acid solution, respectively. As shown in the figures, progressively increase in the fluorescence at 430 nm for 2-hydroxyterephthalic acid, was observed by the illumination of UV light (λ~315 nm) on the nanocubes. Figure 8e further showed that the emission intensity increases with the increasing of the reaction time. The luminescent intensity of the $ZnSn(OH)_6$ is higher than that of the $ZnSnO_3$ because of high concentration of $^{\bullet}OH$ radicals in presence of the $ZnSn(OH)_6$ nanocubes. Moreover, the $Au/ZnSn(OH)_6$ nanocubes exhibited the highest fluorescent intensity in these samples after 120 minutes of reaction time. Because the absorbed wavelength of 2-hydroxyterephthalic acid is located at UV range ($\lambda < 320$ nm, see Figure 8f), this emission was mainly attributed to the $^{\bullet}OH$ radicals that reacted with the terephthalic acid

Dalton Transactions Accepted Manuscript

under visible-light illumination. Therefore, this work demonstrated that the Au NPs decorated nanocubes indeed generated the high concentration of $^{\bullet}OH$ radicals in contrast to the pristine $ZnSn(OH)_6$ and $ZnSnO_3$ nanocubes because of SPR effect. Figure 9a-9b further shows that the PDMS-Au/$ZnSn(OH)_6$ hybrid coating screen exhibited an excellent photodegradation ratio for RB dyes. The hybrid coating screen has successfully simulated a potentially commercial application using Au/$ZnSn(OH)_6$ nanocubes.

4. Conclusion

The $ZnSn(OH)_6$ and Au/$ZnSn(OH)_6$ nanocubes have showed 100% photodegradation ratio under ultraviolet-light within 20 minutes. The cycling test demonstrated high stability of the $ZnSn(OH)_6$ catalyst in the reaction medium without observable loss of photocatalytic activity. The high photodegradation activity is because the hollow $ZnSn(OH)_6$ nanocubes offers high concentration of OH groups to produce a large number of hydroxyl radicals, which are highly active radicals to dissociate the dye molecular. Therefore, the ratio of color lost was still maintained at 100% of the initial rate within 20 mins after five photocatalytic repeated test using $ZnSn(OH)_6$. To the best of our knowledge, this is the fastest photodegradation activity through the $ZnSn(OH)_6$ nanocubes under UV-light, which has never been reported. In addition, after Au decorated $ZnSn(OH)_6$ and $ZnSnO_3$, their absorbance edge was shifted to the wavelength ranging from 450-750 nm. The photodegradation activity under visible-light illumination is following the order: Au/$ZnSn(OH)_6$ > Au/$ZnSnO_3$ >$ZnSn(OH)_6$ > $ZnSnO_3$. The Au/$ZnSn(OH)_6$ nanocubes exhibited the highest photocatalytic activity. This is attributed to that the surface-plasmon induced photoexcited electrons transferred from low energy levels to high energy levels by the interband transitions of the 6 sp electrons of gold to participate in the reaction of photocatalysis. Therefore, the Au/$ZnSn(OH)_6$ nanocubes exhibited an excellent photodegradation ratio of ~ 100% under visible-light illumination. The demonstration of a PDMS-Au/$ZnSn(OH)_6$ hybrid coating screen has further extended its feasible application in our daily life.

Dalton Transactions Accepted Manuscript

Acknowledgements

The authors would like to thank the National Science Council of the Republic of China for financially supporting this research under Contract No. NSC 100-2628-E-035-006-MY2; NSC 102-2221-E-007-146-MY3; NSC 102-2221-E-007-147-MY3.

Figure Captions

Figure 1. FESEM images of (a) $ZnSn(OH)_6$, (b) $ZnSnO_3$ nanocubes, (c) XRD patterns of $ZnSn(OH)_6$ and $ZnSnO_3$ nanocubes. (d) Raman spectra of the $ZnSn(OH)_6$ and $ZnSnO_3$ nanocubes .

Figure 2. Crystallographic structure of (a) $ZnSn(OH)_6$ and (b) $ZnSnO_3$.

Figure 3. (a) Low magnitude of TEM image of the $ZnSn(OH)_6$, (b) High magnitude of the TEM image of the $ZnSn(OH)_6$, (c) HRTEM image of the $ZnSn(OH)_6$ showing the nanocubes separated from each other. (d) HRTEM image showing the lattice fringe of 0.392 nm, which is corresponding to (200) plance of $ZnSn(OH)_6$, inset image is its FFT pattern. (e) Low magnitude TEM image of the $ZnSnO_3$, inset image showing the HRTEM image of the $ZnSnO_3$, the size of the $ZnSnO_3$ nanocubes is ranging from 30 – 80 nm. (f) The corresponding FFT image of the $ZnSnO_3$ nanocubes. (g) Au decorated $ZnSn(OH)_6$ nanocubes. (h) Single crystal Au NPs.

Figure 4. UV-light illumination showing the evolution of a UV-visible absorption spectrum for the 10 μM RB solution of (a) RB solution with $ZnSnO_3$ nanocubes, (b) RB solution with $Au/ZnSnO_3$ nanocubes, (c) RB solution with $ZnSn(OH)_6$ nanocubes, and (d) RB solution with $Au/ZnSn(OH)_6$ nanocubes.

Dalton Transactions Accepted Manuscript

Figure 5. (a) The photodegradation ratio of the $ZnSnO_3$, Au/$ZnSnO_3$, $ZnSn(OH)_6$, Au/$ZnSn(OH)_6$, TiO_2, ZnO, and RB dye. (b) Five photocatalytic cycle tests of the $ZnSn(OH)_6$ nanocubes with RB solution, (c) The PL spectra of the $ZnSn(OH)_6$ and $ZnSnO_3$ nanocubes. (d) The O1s spectra of the $ZnSn(OH)_6$ and $ZnSnO_3$ nanocubes.

Figure 6. (a) Visible-light illumination showing the evolution of a UV-visible absorption spectrum for the 10 μM RB solution of (a) $ZnSnO_3$ nanocubes, (b) Au/$ZnSnO_3$ nanocubes. (c) $ZnSn(OH)_6$ nanocubes, (d) Au/$ZnSn(OH)_6$ nanocubes. (e) The photodegradation ratio of the $ZnSnO_3$, Au/$ZnSnO_3$, $ZnSn(OH)_6$, Au/ $ZnSn(OH)_6$ nanocubes, and blank RB solution. (f) The absorbance spectra with respect to the wavelength of the $ZnSnO_3$, Au/$ZnSnO_3$, $ZnSn(OH)_6$, Au/ $ZnSn(OH)_6$ nanocubes.

Figure 7. Working mechanism for (a) Au/$ZnSn(OH)_6$ under UV-light , (b) Au/$ZnSn(OH)_6$ under visible-light illumination.

Figure 8. Fluorescent property of (a) $ZnSn(OH)_6$, (b) $ZnSnO_3$, (c) Au/$ZnSn(OH)_6$, (d) Au/$ZnSnO_6$, immersing in 5×10^{-4} M terephthalic acid solution under visible-light. (e) The fluorescent intensity as a function of reaction time. (f) The absorbed wavelength of 2-hydroxyterephthalic acid.

Figure 9. (a) UV photodegradation ratio of the PDMS-Au/$ZnSn(OH)_6$ hybrid coating screen (b) The digital image of the hybrid coating screen

References:

1. J. M. Wu and Y. R. Chen, *J Phys Chem C*, 2011, **115**, 2235-2243.
2. X. Chen and S. S. Mao, *Chem Rev*, 2007, **107**, 2891-2959.
3. N. M. Parker, R. J. Psota, A. S. Weber and K. T. Ranjit, *Abstr Pap Am Chem S*, 2007, **233**, 370-370.
4. J. M. Wu, H. C. Shih, W. T. Wu, Y. K. Tseng and I. C. Chen, *J Cryst Growth*, 2005, **281**, 384-390.
5. R. J. Barnes, R. Molina, J. B. Xu, P. J. Dobson and I. P. Thompson, *J Nanopart Res*, 2013, **15**.
6. J. M. Wu, Y. R. Chen and Y. H. Lin, *Nanoscale*, 2011, **3**, 1053-1058.
7. J. M. Wu, H. C. Shih and W. T. Wu, *Nanotechnology*, 2006, **17**, 105-109.

Dalton Transactions Accepted Manuscript

8. J. M. Wu, H. C. Shih, Y. K. Tseng, C. L. Hsu and C. Y. Tsay, *J Electrochem Soc*, 2007, **154**, H157-H160.
9. J. M. Wu, C. W. Fang, L. T. Lee, H. H. Yeh, Y. H. Lin, P. H. Yeh, L. N. Tsai and L. J. Lin, *Journal of the Electrochemical Society*, 2011, **158**, K6-K10.
10. J. M. Wu, Y. R. Chen and W. T. Kao, *Acs Appl Mater Inter*, 2014, **6**, 487-494.
11. J. M. Wu, *J Mater Chem*, 2011, **21**, 14048-14055.
12. L. L. Wang, K. B. Tang, Z. P. Liu, D. K. Wang, J. Sheng and W. Cheng, *J Mater Chem*, 2011, **21**, 4352-4357.
13. Y. C. Pu, G. M. Wang, K. D. Chang, Y. C. Ling, Y. K. Lin, B. C. Fitzmorris, C. M. Liu, X. H. Lu, Y. X. Tong, J. Z. Zhang, Y. J. Hsu and Y. Li, *Nano Lett*, 2013, **13**, 3817-3823.
14. S. T. Kochuveedu, J. H. Oh, Y. R. Do and D. H. Kim, *Chem-Eur J*, 2012, **18**, 7467-7472.
15. S. Linic, P. Christopher and D. B. Ingram, *Nat Mater*, 2011, **10**, 911-921.
16. H. B. Zeng, P. S. Liu, W. P. Cai, S. K. Yang and X. X. Xu, *J Phys Chem C*, 2008, **112**, 19620-19624.
17. Osmando F. Lopes, V. R. d. Mendonç, Ahmad Umar, Mohinder S. Chuahan, Ramesh Kumar, Suvarcha Chauhan and a. C. Ribeiro, *New Journal of Chemistry*, 2015, **39** 4624-4630.
18. D. W. Huang, X. L. Fu, J. L. Long, X. L. Jiang, L. Chang, S. G. Meng and S. F. Chen, *Chem Eng J*, 2015, **269**, 168-179.
19. Y. J. Li and W. Chen, *Catal Sci Technol*, 2011, **1**, 802-809.
20. J. M. Wu, G. K. Hsu, H. H. Yeh and H. C. Lin, *J Electrochem Soc*, 2012, **159**, H497-H501.
21. S. E. H. Etaiw and M. M. El-bendary, *Appl Catal B-Environ*, 2012, **126**, 326-333.
22. X. L. Fu, X. X. Wang, Z. X. Ding, D. Y. C. Leung, Z. Z. Zhang, J. L. Long, W. X. Zhang, Z. H. Li and X. Z. Fu, *Appl Catal B-Environ*, 2009, **91**, 67-72.
23. J. R. Huang, X. J. Xu, C. P. Gu, W. Z. Wang, B. Y. Geng, Y. F. Sun and J. H. Liu, *Sensor Actuat B-Chem*, 2012, **171**, 572-579.
24. J. M. Wu, C. Xu, Y. Zhang and Z. L. Wang, *Acs Nano*, 2012, **6**, 4335-4340.
25. S. T. Kochuveedu, D. P. Kim and D. H. Kim, *J Phys Chem C*, 2012, **116**, 2500-2506.
26. N. Gogurla, A. K. Sinha, S. Santra, S. Manna and S. K. Ray, *Sci Rep-Uk*, 2014, **4**.
27. X. Chen, H. Y. Zhu, J. C. Zhao, Z. T. Zheng and X. P. Gao, *Angew Chem Int Edit*, 2008, **47**, 5353-5356.
28. Z. F. Zheng, J. Teo, X. Chen, H. W. Liu, Y. Yuan, E. R. Waclawik, Z. Y. Zhong and H. Y. Zhu, *Chem-Eur J*, 2010, **16**, 1202-1211.
29. M. J. Yang, C. Hume, S. Lee, Y. H. Son and J. K. Lee, *J Phys Chem C*, 2010, **114**, 15292-15297.
30. K. Ishibashi, A. Fujishima, T. Watanabe and K. Hashimoto, *Electrochem Commun*, 2000, **2**, 207-210.

Dalton Transactions Accepted Manuscript

Figure 1

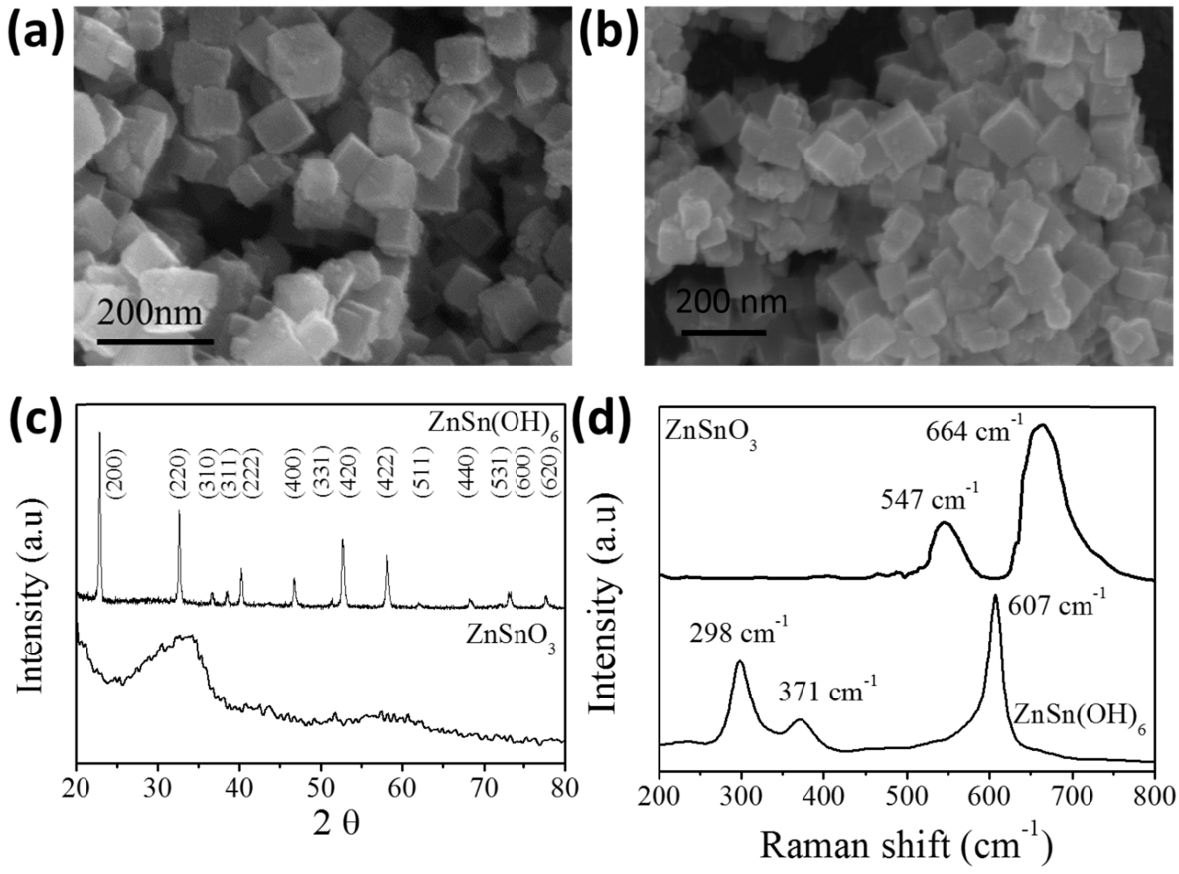

Dalton Transactions Accepted Manuscript

Figure 2

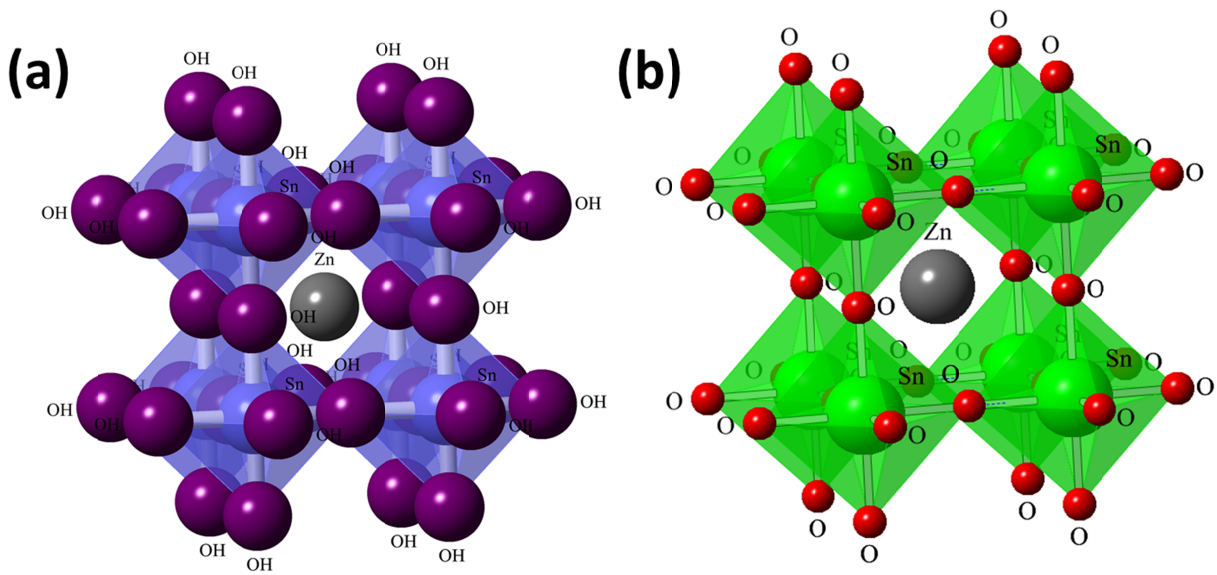

Dalton Transactions Accepted Manuscript

Figure 3

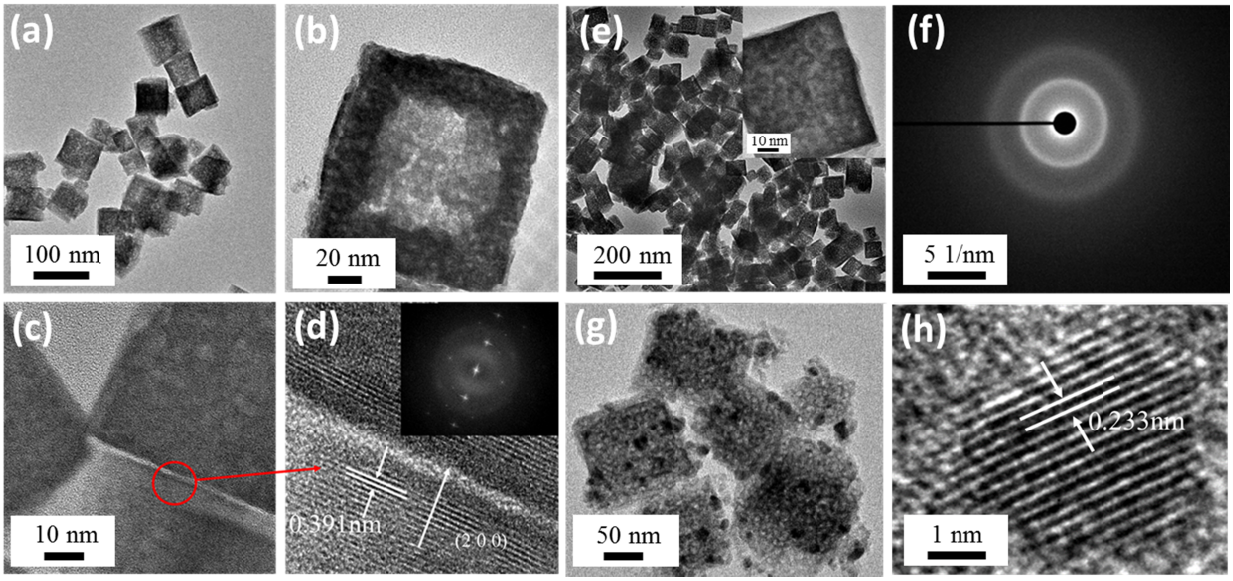

Dalton Transactions Accepted Manuscript

Figure 4

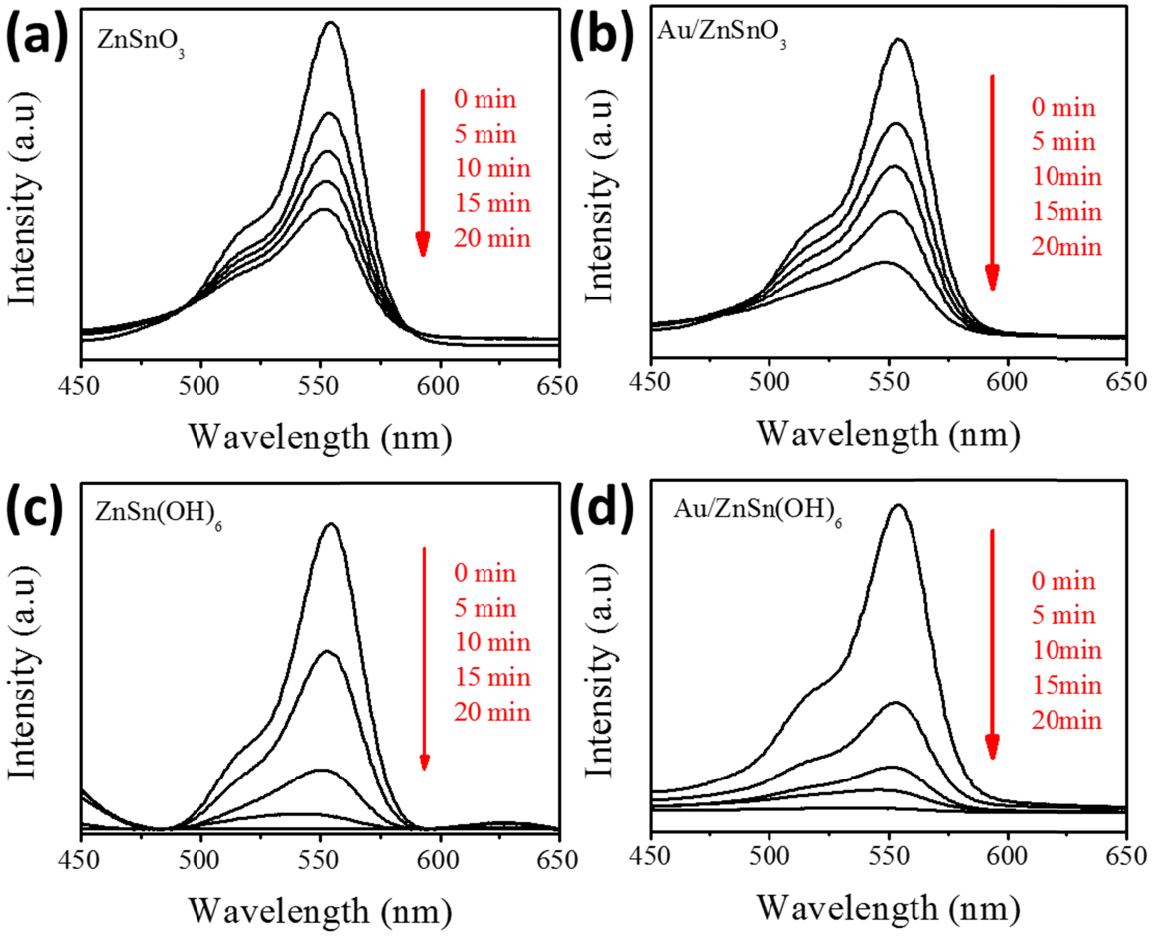

Dalton Transactions Accepted Manuscript

Figure 5

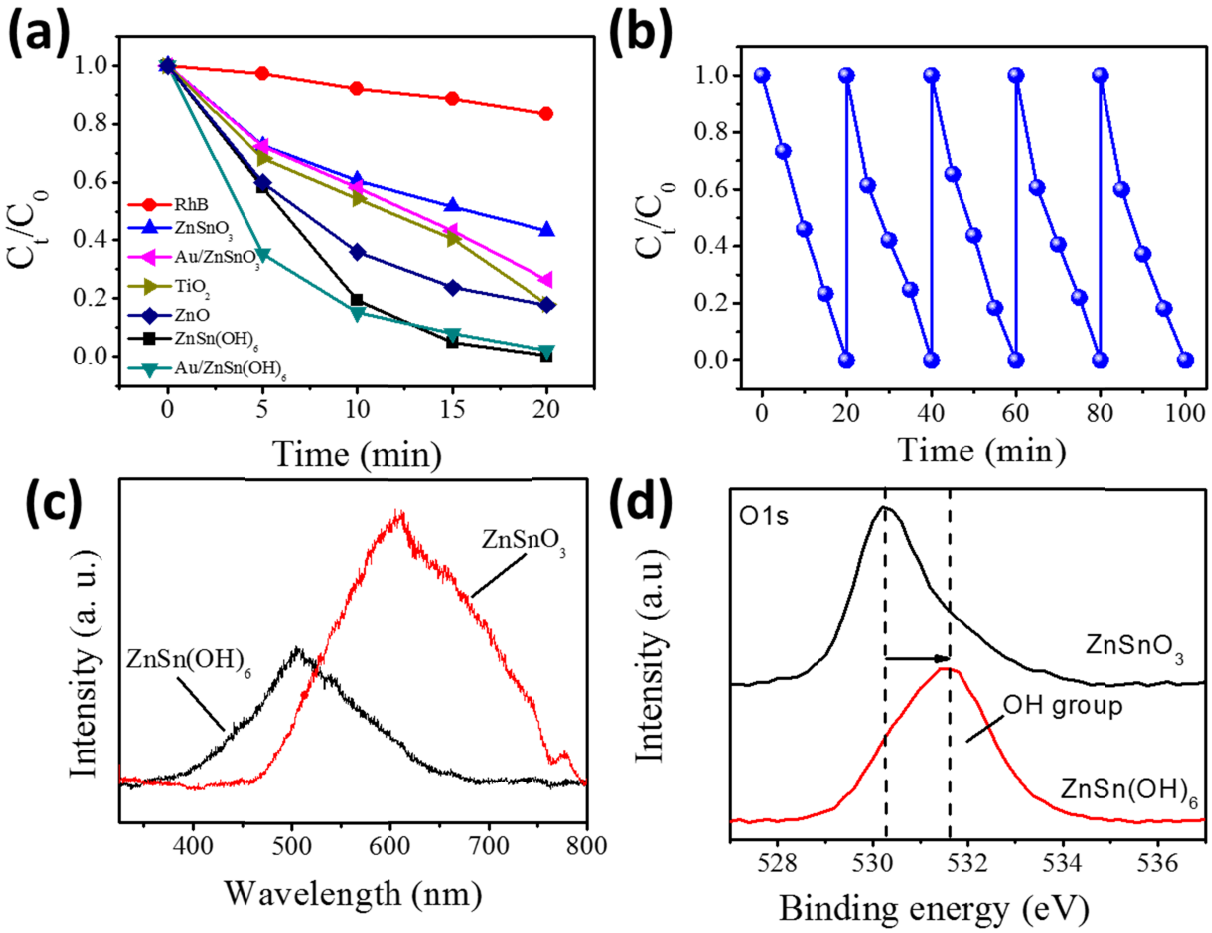

Dalton Transactions Accepted Manuscript

Figure 6

Dalton Transactions Accepted Manuscript

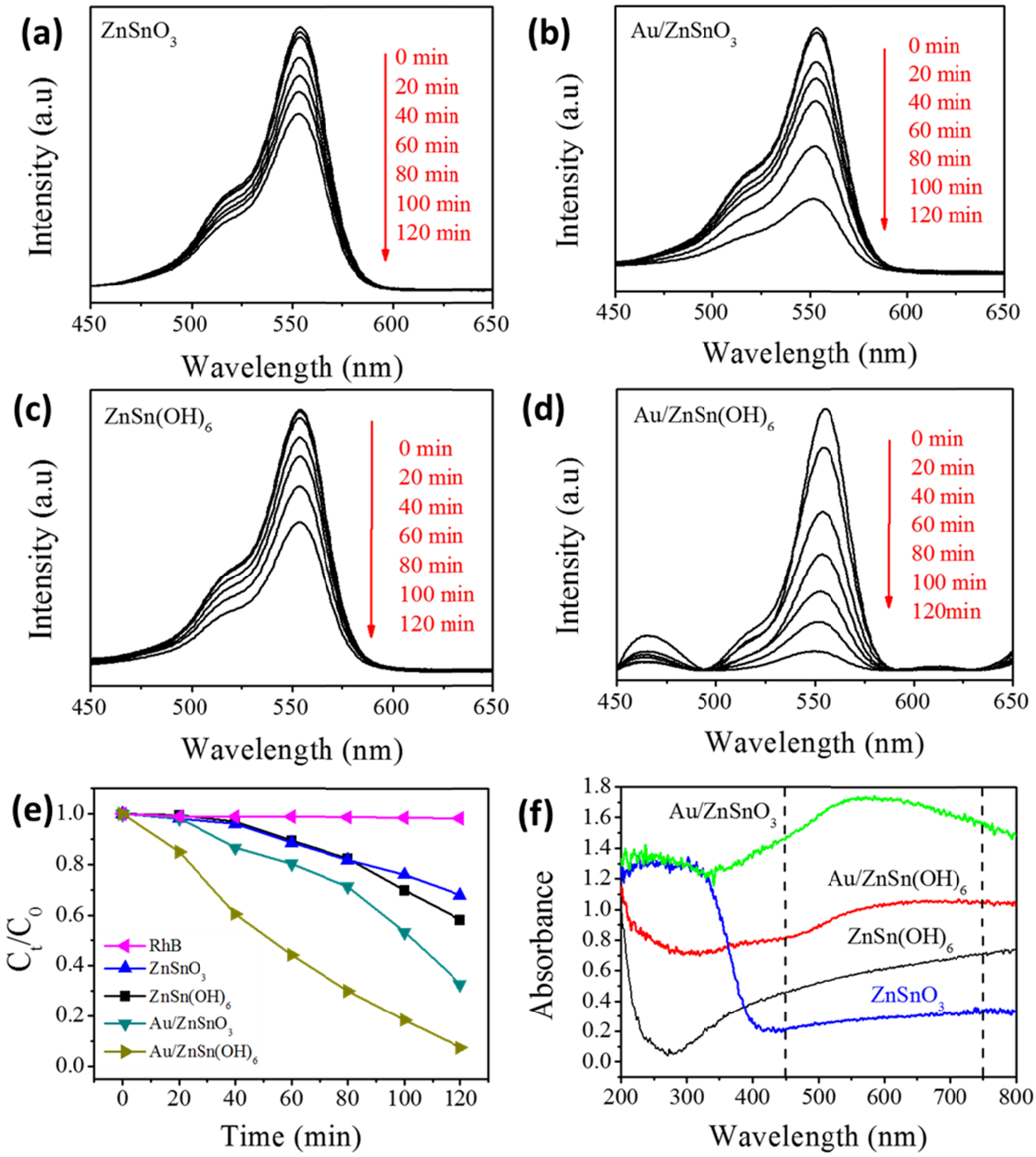

Figure 7

Dalton Transactions Accepted Manuscript

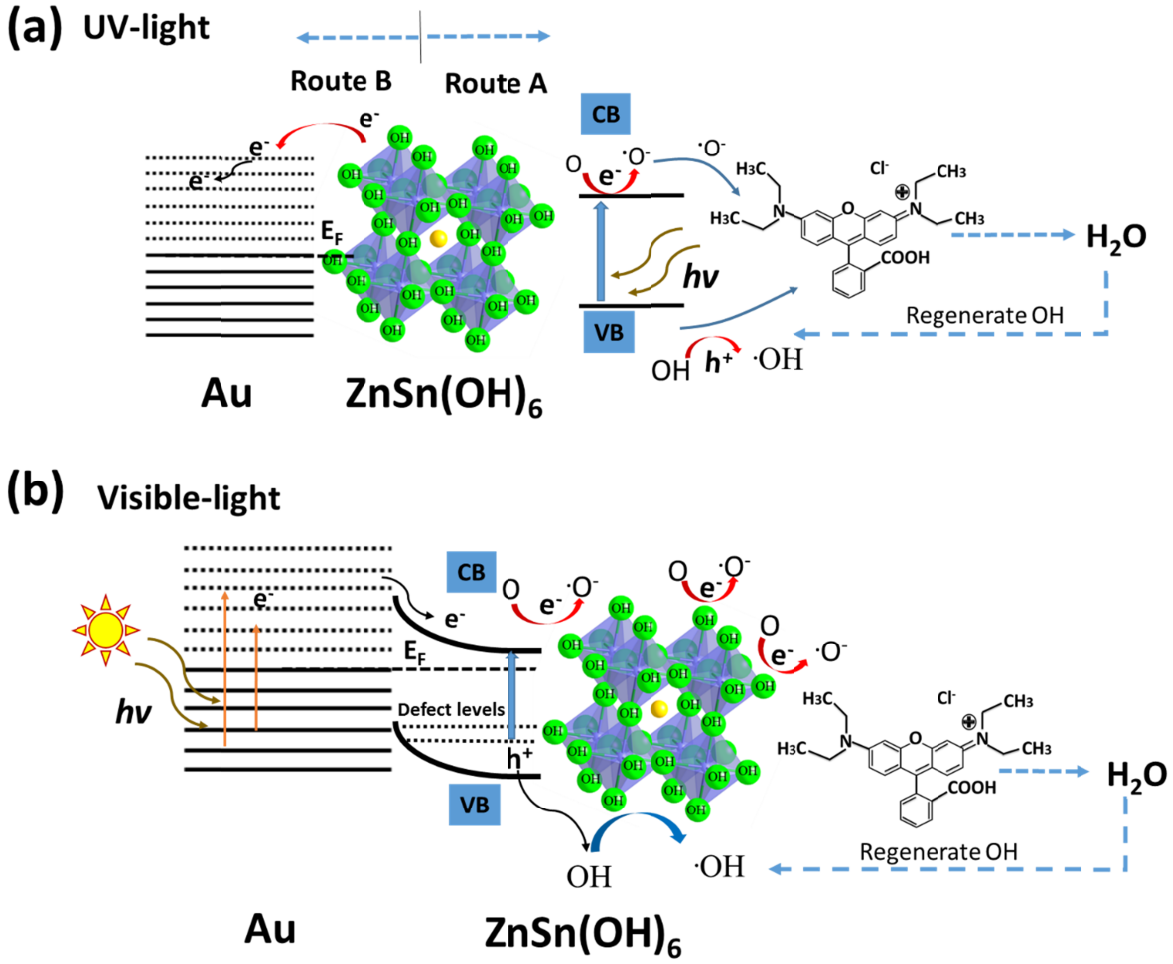

Figure 8

Dalton Transactions Accepted Manuscript

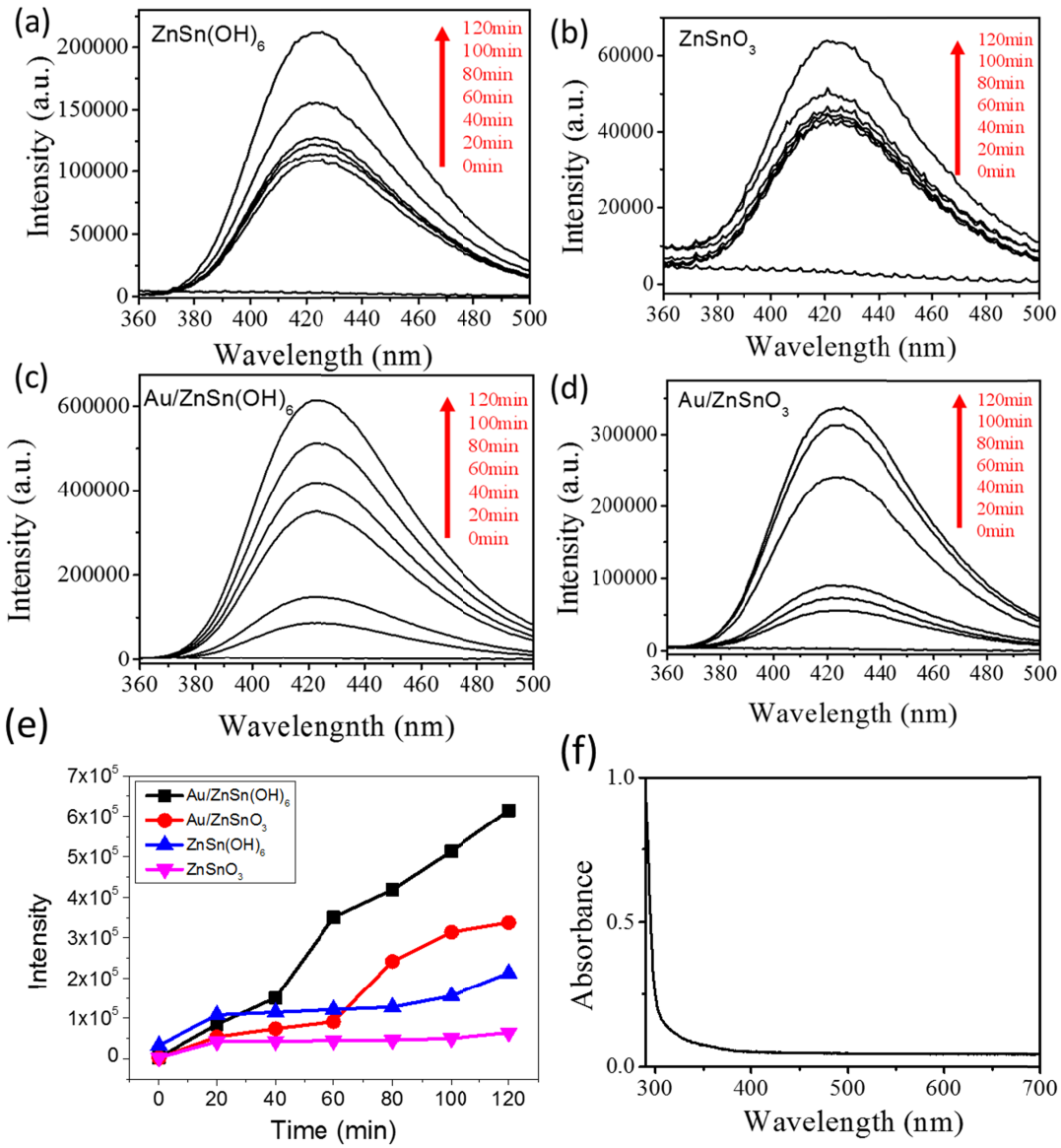

Figure 9

Dalton Transactions Accepted Manuscript

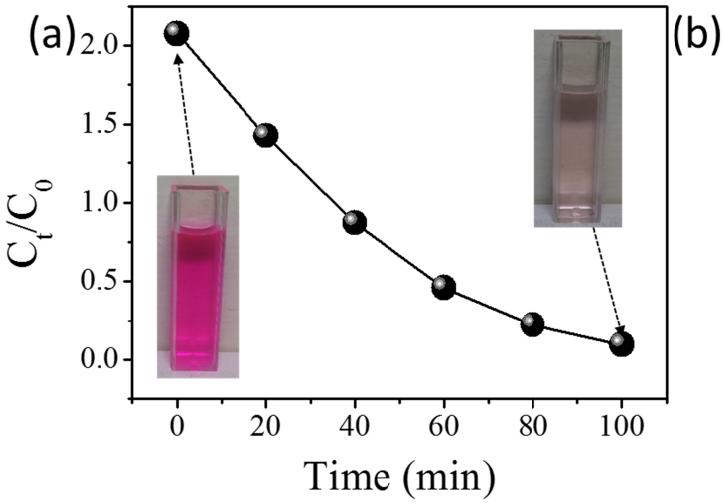

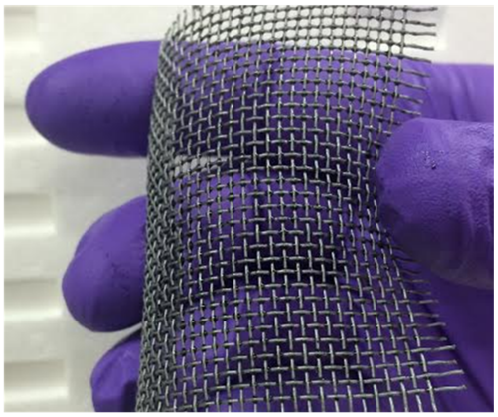

Dalton Transactions Accepted Manuscript